GENETICS

The scales, mechanisms, and dynamics of the genome architecture

Ludvig Lizana[1]* and Yuri B. Schwartz[2]*

Even when split into several chromosomes, DNA molecules that make up our genome are too long to fit into the cell nuclei unless massively folded. Such folding must accommodate the need for timely access to selected parts of the genome by transcription factors, RNA polymerases, and DNA replication machinery. Here, we review our current understanding of the genome folding inside the interphase nuclei. We consider the resulting genome architecture at three scales with a particular focus on the intermediate (meso) scale and summarize the insights gained from recent experimental observations and diverse computational models.

INTRODUCTION

Even when split into 23 chromosomes, 5-cm long each on average, DNA molecules that make up our genomes are too long to fit into the cell nuclei of about 10 μm (10^{-6} m) in diameter unless massively folded. With a diameter of just 2 nm (10^{-9} m), DNA molecules will easily fit in a nucleus considering their mere volume. However, they will be utterly tangled if packed randomly. An attempt to pull out or manipulate a specific stretch of the genome will become almost impossible. However, the cell needs to operate on selected parts of the genome with the transcription factors, RNA polymerases, and DNA replication machinery. Therefore, the real problem is not so much the packing itself but dealing with the entanglements and timely access.

Here, we will review our current comprehension of the genome architecture inside the nuclei resting between cell divisions (interphase nuclei). Confronted by a complex system, humans tend to split it into subcategories. Usually, this helps the understanding but comes with the potential risk of creating a false sense of a strict hierarchy where multiple options are equally likely or when the continuum of dynamic states would be a more truthful representation. With this caveat in mind, we will look at the genome architecture by considering it at three different scales: the microscale, the macroscale, and something between the two, which we will refer to as the mesoscale. The architecture at micro- and macroscales is relatively stable and corresponds to structures detectable by biochemical and microscopy methods. In contrast, the mesoscale architecture is notably more dynamic and represented by probabilistic folding patterns rather than stable structures. The probabilistic patterns are more difficult to study because they are often altered by the experiment itself. However, because of its dynamic nature, the genome folding at this scale may be the most relevant for gene regulation.

THE GENOME ARCHITECTURE AT MICRO- AND MACROSCALES

Nucleosomes are central to the microscale of the genome folding. Formed by the electrostatic interactions between the DNA and the particle made of four pairs of histone proteins, nucleosomes reduce the linear size of genomic DNA approximately sixfold (Fig. 1). The crystal structure of an isolated nucleosome was mapped to the atomic detail and, therefore, is well understood (*1*, *2*). Recent attempts to look at nucleosomes inside the cells using cryo–electron microscopy suggest that structures of some or even many of them deviate from the "canonical" structure above (*3*, *4*). Nevertheless, these deviations are relatively minor. Overall, at the microscale, the genome emerges as the "beads-on-a-string" fiber composed of nucleosomes connected by short DNA linkers often referred to as the "10-nm fiber."

Although relatively stable, the 10-nm fiber is neither static nor entirely uniform. Recent advances in the application of high-throughput sequencing technologies to study the nucleosome arrangement suggest substantial variation in the nucleosome occupancy, positioning, and spacing at different genomic locations. Here, we refer to the nucleosome occupancy as a metric of how often a genomic position is present within a nucleosome particle. The positioning specifies how consistently nucleosomes are placed relative to a specific DNA sequence, and the spacing describes the distance between the dyads of two neighboring nucleosomes. The nucleosome arrays downstream of transcription start sites of transcriptionally active genes tend to be strongly positioned with less regular spacing. In contrast, the nucleosome arrays within transcriptionally inactive loci display poor positioning but regular spacing (*5*, *6*). Nucleosome occupancy, positioning, and spacing are regulated by action of a dedicated class of adenosine triphosphate (ATP)–dependent nucleosome remodeling factors. Some of these factors catalyze nucleosome sliding on DNA; others evict nucleosomes. We refer the interested reader to recent reviews for in-depth discussion of nucleosome array arrangements and ATP-dependent chromatin remodeling (*7*, *8*).

At the macroscale, we consider the genome at the level of individual chromosomes, which appear as distinct territories (Fig. 1). The term was coined by Theodor Bovery early in the 20th century to describe individual volumes occupied by interphase chromosomes [for a detailed review of the subject, see (*9*)]. After the emergence of chromosome-specific fluorescent in situ hybridization (FISH) probes and the development of three-dimensional (3D) FISH assays, the existence of chromosome territories is well established (*10*–*12*). Ample experimental evidence indicates that the positions of individual chromosome territories are not random. Thus, in the cells with spherically shaped nuclei, gene-rich chromosomes are positioned in the nuclear interior compared to the more peripheral position of gene-poor chromosomes (*13*–*15*). Although, for the flat-ellipsoid nuclei (e.g., in fibroblasts), the radial arrangement of chromosome territories correlates best with their size (*10*), on the sub-chromosomal level, the local gene density within 2 to 10 million base pair (Mb)

[1]Integrated Science Lab, Department of Physics, Umeå University, Umeå, Sweden. [2]Department of Molecular Biology, Umeå University, Umeå, Sweden.
*Corresponding author. Email: ludvig.lizana@umu.se (L.L.); yuri.schwartz@umu.se (Y.B.S.)

segments still appears as the key predictor of their radial position (*14*, *16*, *17*). It is less clear whether, in addition to nonrandom radial positions, territories of specific chromosomes occupy particular positions with respect to each other as conflicting evidence exists to support (*18*–*20*) or refute (*10*, *21*) this hypothesis.

While the nonrandom position of individual chromosome territories is unexpected, even more unexpected is that individual chromosomes do not mix. According to standard polymer physics, a dense polymer solution, like chromatin in the nucleus, should interpenetrate and entangle when in thermodynamic equilibrium (*22*). To better understand the basic principles for polymer mixing, consider a simple polymer model (*23*) with identical monomers (homopolymer) that cannot overlap each other (so-called excluded-volume interactions). To determine the mixing behavior, we define two critical volume fractions: polymer volume fraction (ϕ_p) and overlap volume fraction (ϕ_o). The polymer volume fraction ϕ_p is the sum of all monomer volumes V_p (or the "tube" volume) divided by the enclosing volume V_s (solvent volume). The volume fraction ϕ_p differs slightly from the overlap volume fraction ϕ_o, which relates the polymer's tube volume V_p to the volume spanned by an equilibrated polymer, called pervaded volume V_{per}, rather than the solvent volume Vs (Fig. 2A, blue-shaded circles). Mathematically, we define these volume fractions as

$$\phi_p = \frac{V_p}{V_s} \text{ and } \phi_o = \frac{V_p}{V_{per}}$$

These two ratios grow differently depending on polymer length. To see how, we first estimate the pervaded volume through the polymer's radius of gyration R_G, where $V_{per} \sim R_G^3$. Next, if denoting the number of monomers as N and their radius by b, then $R_G \sim bN^{0.588}$ or $V_{per} \sim b^3N^{3\times0.588} = b^3N^{1.764}$ [the exponent 0.588 is associated with a self-avoiding homopolymer; (*23*)]. This scaling behavior differs from the polymer's tube volume, where $V_p \sim b^3N$. On the basis of these relations, the volume fractions above become

$$\phi_p \sim \frac{b^3}{V_s} \times N \sim N \text{ and } \phi_o \sim N^{-0.764}$$

For growing N, we note that ϕ_p increases, whereas ϕ_o decreases, and that there is a critical polymer length (or monomer density) where $\phi_p = \phi_o$. Because chromatin fibers are so long ($N \gg 1$), we have $\phi_p \gg \phi_o$.

Figure 2 illustrates the mixing regimes based on relative proportions between ϕ_p and ϕ_o when there are several polymers in the solution. The first regime is the dilute polymer solution where $\phi_p < \phi_o$ (Fig. 2A). Here, the total polymer concentration is low, and the pervaded volumes do not overlap (shaded circles). If increasing the concentration by adding more polymers (or making the ones in the solvent longer), the volume fraction ϕ_p grows until $\phi_p \approx \phi_o$ (Fig. 2B). Here, the polymers begin to invade each other's pervaded volumes and mark the transition to the mixed regime (called semi-dilute in polymer physics). Because, in the nuclei of eucaryotic cells, the overlap fraction is small ($\phi_p \gg \phi_o$) (thin and very long chromatin fibers), polymer physics predicts that, in thermodynamic equilibrium, chromosomes will be mixed (Fig. 2C). However, in the cell nuclei, the fibers of interphase chromosomes avoid entangling and, instead, form chromosome territories.

What prevents the interphase chromosomes from mixing? The main mixing mechanism for linear polymers is reptation, where the ends penetrate the globule like slithering snakes. As shown computationally (*24*), for long polymers, the reptation is very slow. Moreover, telomeric regions of chromosomes tend to interact with each other and the nuclear membrane and thereby constrain the mobility of the

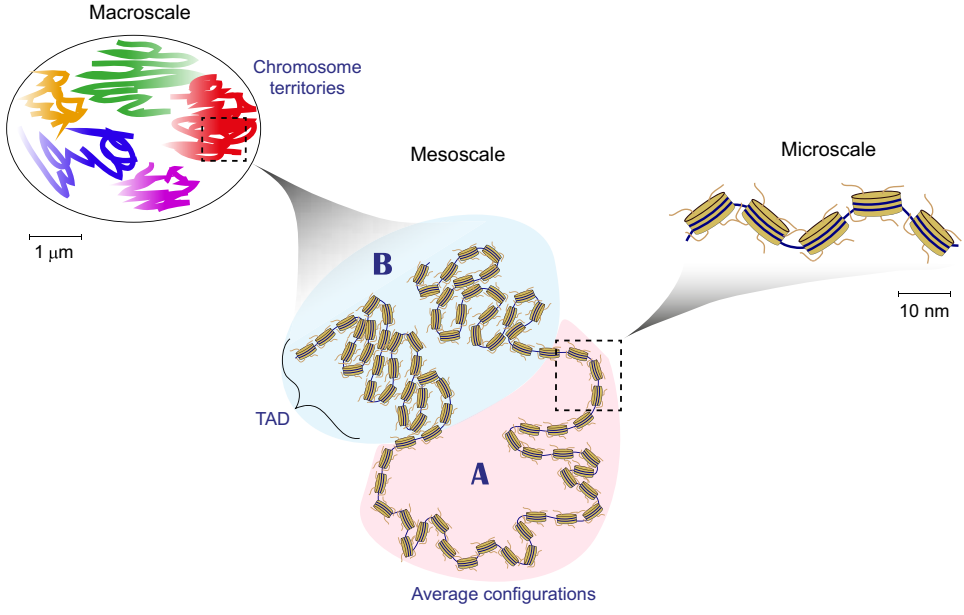

Fig. 1. The genome architecture scales. At the microscale, DNA is wrapped around the 10-nm particle made of four pairs of histone proteins, which reduces the linear size of genomic DNA approximately sixfold. At the macroscale, each chromosome occupies its own territory (shown schematically in different colors). The mesoscale architecture is represented by probabilistic folding patterns among which the most common are topologically associated domains (TADs) and A and B compartments (illustrated as shades of red and blue).

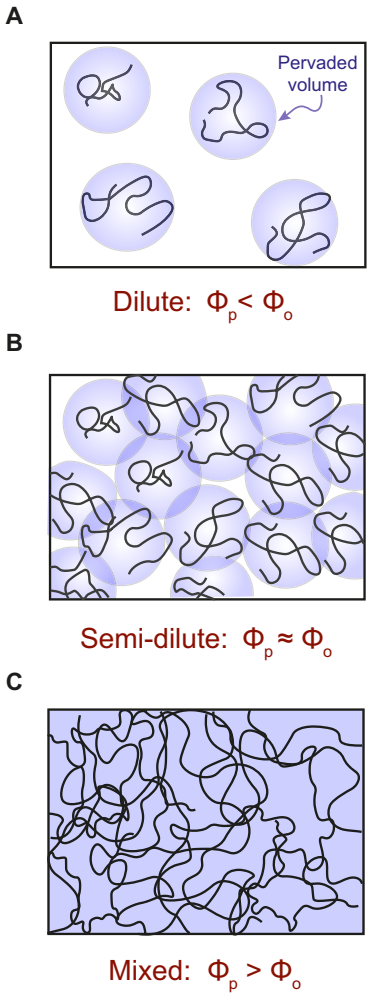

Fig. 2. Polymer mixing regimes at equilibrium. (**A**) Dilute solution. The concentration is so low that polymers do not overlap with each other's pervaded volumes (blue shades). (**B**) Semi-dilute regime. When reaching a critical polymer concentration, the pervaded volumes begin to overlap. (**C**) Mixed regime. The polymer density is so high that the pervaded volumes overlap substantially—the polymers mix.

chromosome ends even further. Slow reptation means that, although not strictly forbidden, the mixing of the interphase chromosomes, after they emerge from the ultracompact state associated with cell division, requires a very long time. This time is orders of magnitude longer than the lifetime of a typical cell. To prove this point, Halverson and coauthors (*22*) compared the mixing behaviors of a concentrated solution of short linear polymers (high reptation) to that of a concentrated solution of the same-size polymers whose ends are joined to form non-catenated rings (reptation forbidden). Extensive simulations show that, while linear polymers fully mix, the ring polymers segregate into chromosome-like territories (*22*).

The insight that interphase chromosomes correspond to nonequilibrium polymers that obey three basic rules (they are compact, knot-free, and unable to cross itself) sparked an interest in geometries that conform to these constraints. Theoretical work to address this question led to the fractal (or crumpled) globule model of interphase chromosomes (*25*). Realizations of crumpled globule conformations are known in mathematics as space-filling curves, for example, the Hilbert curve and its closed-loop version called the Moore curve. As we discuss in the following section, the frequency of chromosomal contacts between two loci decays with the distance that separates them. The fractal globule model predicts that the contact probability between two polymer segments separated by the distance l should decay as $1/l$. While there are substantial variations between individual loci and cell types, the experimental measurements suggest that the average decay in the frequency of chromosomal contacts in human cells does follow this rule (*26*).

Curiously, in certain insects, for example *Drosophila melanogaster*, the two homologous chromosomes form a joint chromosome territory due to the process called somatic pairing. The mechanism that appears to override the topological constraints that prevent chromosome territories from merging in this case is not well understood. We refer the interested reader to a comprehensive review (*27*) and two recent investigations of this fascinating phenomenon (*28*, *29*).

THE GENOME ARCHITECTURE AT MESOSCALE

Despite the immense progress of the last decade, our understanding of the genome architecture between the microscale and the macroscale is still rapidly evolving (Fig. 1). Cryo–electron microscopy, electron microscopy tomography combined with DNA labeling (ChromEMT), and chromatin expansion microscopy (ChromExM) suggest that the beads-on-a-string fiber folds into disordered chains of variable diameters (*30*–*33*). These chains have different local nucleosome arrangements and structural conformations with local chromatin volume concentrations that vary between 12 and 52%.

A different view of the genome architecture at the mesoscale is provided by the chromosome conformation capture (3C) approach (*34*), and its nonselective high-throughput Hi-C version (*26*) has been particularly influential. The 3C approach is based on the idea that the relative special proximity of any two genomic regions can be deduced from the ease with which these fragments are joined together by the DNA ligase. In a Hi-C assay, the live cells are cross-linked by a short treatment with formaldehyde, their genome cut into fragments, and these fragments are ligated under conditions that favor ligation between the fragments in close spatial proximity. The ligation junctions are then identified by sequencing. We refer the reader to recent reviews devoted to technical details of the 3C assays (*35*, *36*). It is important to underscore that Hi-C measures the frequencies with which any two genomic sites are joined together. Therefore, it requires pools of hundreds of thousands to millions of cells, and its outcome is an average over a large cell population. Hi-C analyses of genomic contacts in multiple cell types from a plethora of different species established that the frequency of chromosomal contacts decays following a power law with a scaling exponent that is close to −1 (Fig. 3A) (*26*, *37*). They confirm that the genome folding is not uniform and displays two major kinds of contact patterns. The first kind, dubbed topologically associated domains (TADs) (*38*), corresponds to broad domains (up to 1 Mb) with similar contact frequencies, which decay slowly until the edge of the domain (Fig. 3B). At TAD edges, the contact frequencies drop more abruptly, although rarely more than twofold. The small magnitude of the drop presents a challenge for detection, and, hardly unexpected, different computational methods for TAD detection often return substantially different results (*39*, *40*). The second kind of contact pattern represents longer-range interactions between chromosomal regions, referred to as "A" and "B" compartments (Fig. 3B) (*26*). The A compartment regions tend to be gene-rich and contain a

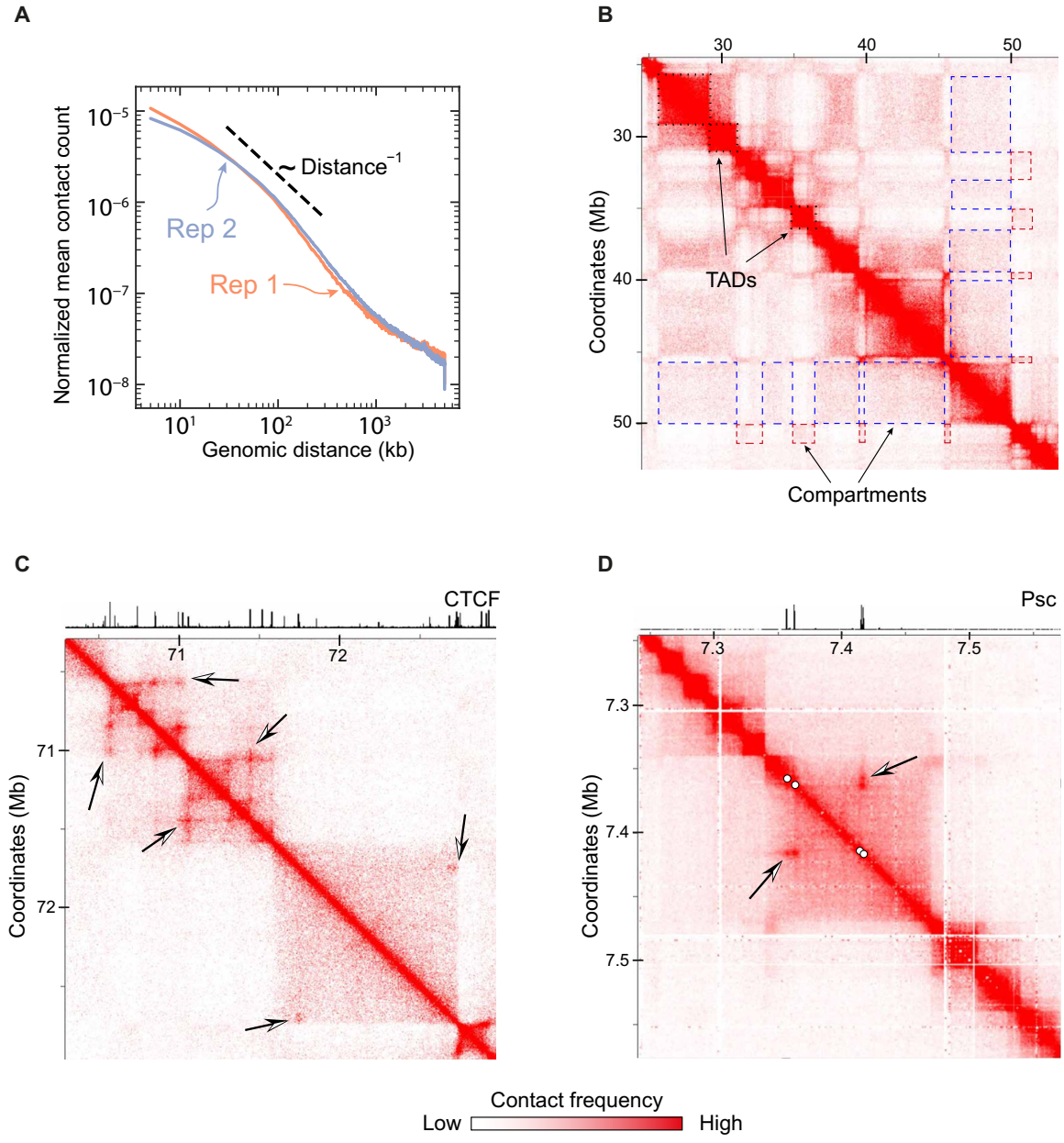

Fig. 3. Genomic contact patterns detected by Hi-C. (**A**) The average number of contacts between 5-kb segments of the *D. melanogaster* chromosome arm 2L, measured by two independent experiments [blue and orange curves; data from (*81*)], was normalized to the total number of detected contacts and plotted as a function of the distance between the segments. The dashed line illustrates the expected frequency of genomic contacts when they decay following a power law with a scaling exponent −1 as measured in human cells. Note that, for the *Drosophila* genome, the value of the scaling exponent is slightly different with positive deviations for small and large distances (*37*). (**B**) The heatmap representation of contact frequencies along a segment of human chromosome 14 (*46*) illustrates two major kinds of contact patterns: TADs (which appear as squares along the heatmap diagonal, three representatives marked with dotted lines), and longer-range interactions dubbed A-B compartments. These appear as pale checker-board patterns (representative compartments marked with blue and red dashed squares). (**C**) The heatmap of contact frequencies within a small region of human chromosome 8 illustrates spatial proximity between sites bound by the CTCF protein. Those appear as dots, some of which are marked with arrows. Chromatin immunoprecipitation sequencing (ChIP-seq) signals for CTCF (*152*) are shown above the heatmap to mark the location of the binding sites. (**D**) Likewise, the four PREs from *invected-engrailed* locus [marked by the ChIP-seq signal peaks for the Polycomb group protein Psc (*153*), and white circles on the heatmap diagonal] appear as dots (indicated with arrows) on the contact map of *Drosophila* chromosome 2R (*48*). Contact heatmaps in (B) to (D) were plotted using Juicebox.js (*154*).

large fraction of transcriptionally active genes. In contrast, the regions from the B compartment tend to be gene-poor and transcriptionally inactive.

Aside from TADs and A/B compartments, the Hi-C–type methods detect features known from cytological observations, e.g., preferential contacts between telomeres, clustering of centromeres (*37*), and higher-than-expected contacts between loci repressed by the Polycomb system (*41*–*45*). The regions above are relatively large with a size range of tens to hundreds of thousand base pairs (kb). In addition, Hi-C detects spatial proximity between certain short (~1 kb) regions (Fig. 3, C and D). The latter includes a subset of mammalian CCCTC-binding factor (CTCF) binding sites (*46*, *47*), some *Drosophila* Polycomb response elements (PREs) (*48*, *49*), and certain transcriptional enhancers and "promoter-proximal tethering elements" (*50*). While plausible explanations of increased proximity between CTCF binding sites and PREs are provided by computer modeling (see the "The insights from nonequilibrium models" section for details), the mechanistic understanding of the promoter-proximal tethering elements requires further investigation (*51*).

Two recent sequencing-based assays, genome architecture mapping (*52*) and split-pool recognition of interactions by tag extension (SPRITE) (*53*), further expanded our view of the mesoscale genome architecture. Unlike the 3C, these assays do not rely on proximity ligation and may detect multiple DNA interactions that occur simultaneously within the nucleus. Moreover, SPRITE can be adapted to detect DNA-RNA interactions (*54*). In addition to TADs, A-B compartments, and pointed contacts observed by Hi-C, SPRITE uncovered the preferential localization of transcriptionally inactive regions close to the nucleoli (nuclear bodies encompassing ribosomal RNA genes) (*55*) and highly transcriptionally active regions in closer proximity to the nuclear speckles (nuclear bodies that contain proteins involved in mRNA splicing and processing) (*56*).

Super-resolution microscopy methods such as stochastic optical reconstitution microscopy or 3D structured illumination microscopy to name a few [for recent review, see (*57*)] combined with automated in situ hybridization of fluorescently labeled synthetic oligonucleotide probes (*58*) provided complementary approaches to trace genome folding at the mesoscale. Inherently single-cell techniques, these chromosome tracing approaches provided a critical missing piece of the puzzle to settle the molecular nature of TADs. On the one hand, traces of individual chromosomes displayed globular folded structures dubbed "TAD-like domains" (*59*) or "chromatin nanodomains" (*60*). However, their number and boundaries varied considerably between individual cells (*59*–*62*), so these structures should not be equated with TADs. On the other hand, when averaged over multiple cells, chromosome tracing reproduced proximity patterns matching TADs detected by Hi-C (*59*, *60*, *63*, *64*). This argues that TADs represent statistical patterns emerging from the dynamic motion of chromatin polymer rather than stable formations. To what extent the "TAD-like" or "nanodomains" correspond to the variable local nucleosome arrangements detected by ChromEMT or ChromExM is an interesting open question.

DNA ELEMENTS WITH IMPACT ON GENOME ARCHITECTURE

Several kinds of DNA elements have been linked to nonuniform genome folding at the mesoscale. Some of them drive processes that require access to the DNA, for example, transcription, so their effects on the genome folding are circumstantial. However, a class of DNA elements, dubbed chromatin insulators, seems to have evolved for their ability to constrain chromatin contacts across. These elements were discovered in *Drosophila* (*65*–*67*) and subsequently identified in several developmental genes of flies and vertebrates (*68*–*74*). At first, chromatin insulators were operationally defined as DNA elements that block the activation of a promoter by a transcriptional enhancer element when placed between the two. In contrast to transcriptional repression, the insulation leaves the promoter competent for activation by any other enhancer that is not separated from the promoter by the insulator element. Several *Drosophila* proteins, including Suppressor of hairy wing, Centrosomal protein 190kD, Modifier of mdg4, and CTCF, have been discovered in genetic screens for components required for insulators to block enhancer-promoter "communication." This list was further expanded by biochemical studies of their interaction partners [reviewed in (*75*)]. From these *Drosophila* proteins, only one, CTCF, has a clear ortholog in vertebrates.

Overall, only a handful of proteins, namely, CTCF and its interacting partners DEAD-box RNA helicase p68 (DDX5) (*76*) and Myc-Associated Zinc Finger protein (MAZ) (*77*, *78*), have been implicated as insulator factors in vertebrates compared to more than a dozen proteins associated with insulation in *Drosophila* (*75*). It was proposed that flies may have evolved a more diverse set of insulator elements and associated proteins because their genome is an order of magnitude smaller albeit it contains nearly the same number of genes and, therefore, has a greater need to constrain 3D interactions. This is an interesting hypothesis worth further testing. Alternatively, many vertebrate insulator proteins may still await to be discovered. Perhaps, flies owe their extensive catalog of insulator proteins to ingenious transgenic systems that enabled genetic screens.

Many genomic sites that bind combinations of *Drosophila* insulator proteins block enhancer-promoter communication (*79*, *80*), limit genomic contacts across (*81*), and overlap with TAD borders (*37*, *81*, *82*). However, the binding of known insulator proteins, individually or in combination, does not predict whether a site corresponds to a functional insulator element (*79*, *80*). Perhaps, additional yet unknown proteins or specific chromatin context must be accounted for to enable accurate predictions. Likewise, not all mammalian CTCF binding sites act as chromatin insulators. However, those that do co-bind cohesin complexes and often display "stripe" contact patterns in Hi-C assays, which indicate preferential interactions of these sites with broad stretches of adjacent chromatin (*83*, *84*). The DNA sequence motif recognized by CTCF is not palindromic and, therefore, has an orientation. A pair of neighboring CTCF binding sites on the same chromosome can have four possible orientations of corresponding sequence motifs: the same direction on one strand, the same direction on the other strand, convergent motifs on opposite strands, and divergent motifs on opposite strands (Fig. 4). Notably, 92% of CTCF-bound region pairs within the human genome displayed convergent sequence motifs (*46*). When these pairs of CTCF regions also co-bind cohesin complexes, they show substantially closer proximity with one another than with the loci lying between them, which is seen as distinct "dots" on Hi-C contact maps (*46*). First interpreted as stable chromatin loops, the dots were later understood to be probabilistic features that emerge due to the ability of chromatin-bound CTCF to stall cohesin-mediated chromatin loop extrusion (*85*–*88*). We will return to this process later in the review. In contrast to mammalian CTCF-dependent insulators, *Drosophila* CTCF binding sites show no genomic preference in the orientation of the underlying recognition sequences (*89*), although the recognition

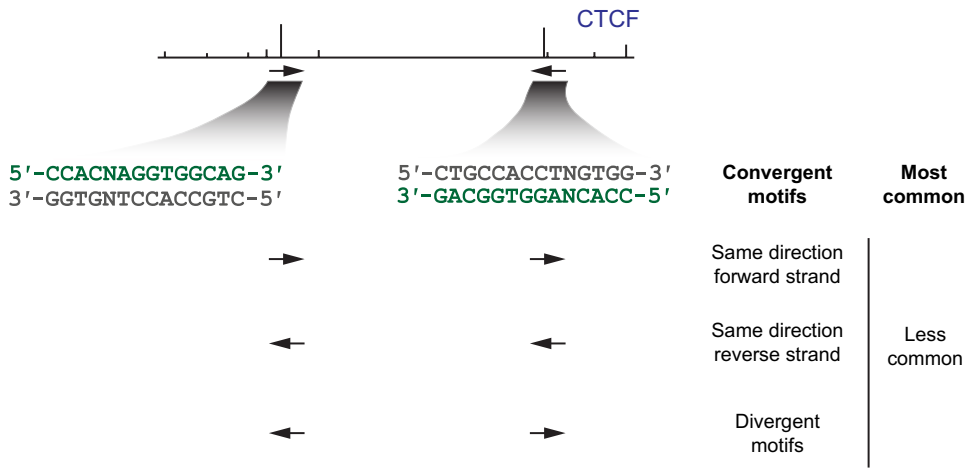

Fig. 4. Orientation bias of CTCF recognition sequences. The sequence motif recognized by CTCF (the consensus sequence is shown underneath the cartoon illustrating the CTCF binding profile) is asymmetric. A pair of binding sites may have four possible orientations of the corresponding recognition sequences (indicated with black arrows). Notably, the majority of the CTCF-bound region pairs within the human genome have recognition motifs in the convergent orientation.

sequence itself is evolutionarily conserved. Furthermore, *Drosophila* insulator elements impair chromatin contacts without displaying stripe or "loop-dot" contact patterns (*50*, *81*), which would be expected if they block chromatin contacts generated by loop extrusion. How *Drosophila* insulators affect genome folding at the molecular level remains a mystery.

Although fly insulator elements do not display loop-dot contact patterns, several hundreds of "loop-dots" are detected in the high-resolution *Drosophila* Hi-C maps (*48*–*50*, *90*). These dots correspond to three kinds of regions: PREs, a group dubbed distal tethering elements, and meta-loop anchors. PREs are the short (~1 kb) DNA elements that correspond to high-occupancy binding sites for so-called Polycomb group proteins. These proteins act together as repressive complexes, which bind many key developmental genes and use post-translational methylation of histone H3 at lysine-27 to epigenetically repress alternative gene expression programs in differentiated cells (*91*). Distal tethering elements were suggested to facilitate interactions between promoters and distal enhancers (*50*, *51*) although their role and mechanism of action require further studies. Meta-loop anchors are the most recently discovered group of elements that appear to increase the spatial proximity between certain neural gene promoters and intergenic accessible chromatin sites located million base pairs apart (*90*). Like all loop-dots, the "meta-loops" are likely probabilistic, so far detected only in the cells of the *Drosophila* central nervous system.

THE INSIGHTS FROM COMPUTATIONAL MODELING OF THE GENOME FOLDING AT EQUILIBRIUM

Rare for biology, our understanding of the mechanisms behind the genome architecture at the mesoscale is strongly influenced by theoretical studies. Usually, these studies start by modeling mathematical polymers: linear chains of equally sized monomers representing a short chromatin segment, typically 1 to 10 nucleosomes long (*92*). Depending on the coarse-graining level, from 450 to 4500, such monomers are required to explore the folding of a genome stretch representing an average-sized mammalian TAD.

Most modeling approaches can be grouped into two primary categories: equilibrium and nonequilibrium models [for a dedicated review of the subject, see (*93*–*95*)]. Equilibrium models focus on interaction energies between different polymer sections and the effect of corresponding interactions on the polymer conformation in the equilibrium. In contrast, nonequilibrium models envision the polymer responding to local stochastic forces. These forces are assumed to use some external energy source (e.g., ATP hydrolysis) to continuously push the system out of equilibrium. While the two approaches are implemented using distinct theoretical frameworks, they agree on some of the predictions. For example, both equilibrium and nonequilibrium models have parameters that can be tuned to match and reproduce major contact patterns observed by Hi-C. Below, we review key features and insights gained from both kinds of approaches starting from equilibrium models.

One of the most popular equilibrium frameworks is the strings-and-binders-switch (SBS) model (Fig. 5A) (*96*). The SBS model represents chromatin as a self-avoiding polymer chain with binding sites that may associate with freely diffusing beads, representing DNA binding proteins. Besides binding to the polymer, these beads also form dimers. Therefore, while staying attached to the polymer, two beads may come in contact due to the polymer fluctuations and create a molecular bridge that constrains the polymer motion. If the concentration of the binder molecules is sufficiently high, then the polymer collapses via coil-to-globule transition. By adjusting the SBS model parameters, the original study reproduced reported chromatin folding scaling properties, fractal states, domain formation, and critical loops. The initial SBS framework has inspired numerous extensions and applications (*93*, *94*); for example, improving the fit of Hi-C data (*97*), studying the folding of specific loci (*98*), isolating essential enhancer-promoter contacts (*99*), and offering a better understanding of the relations between bridging, folding, and transcriptional activity (*100*).

One may argue that it is unnecessary to include binder molecules in the simulations. Instead, it may be enough to consider a polymer chain composed of blocks with different properties that interact with each other. This is the underlying assumption of block copolymer

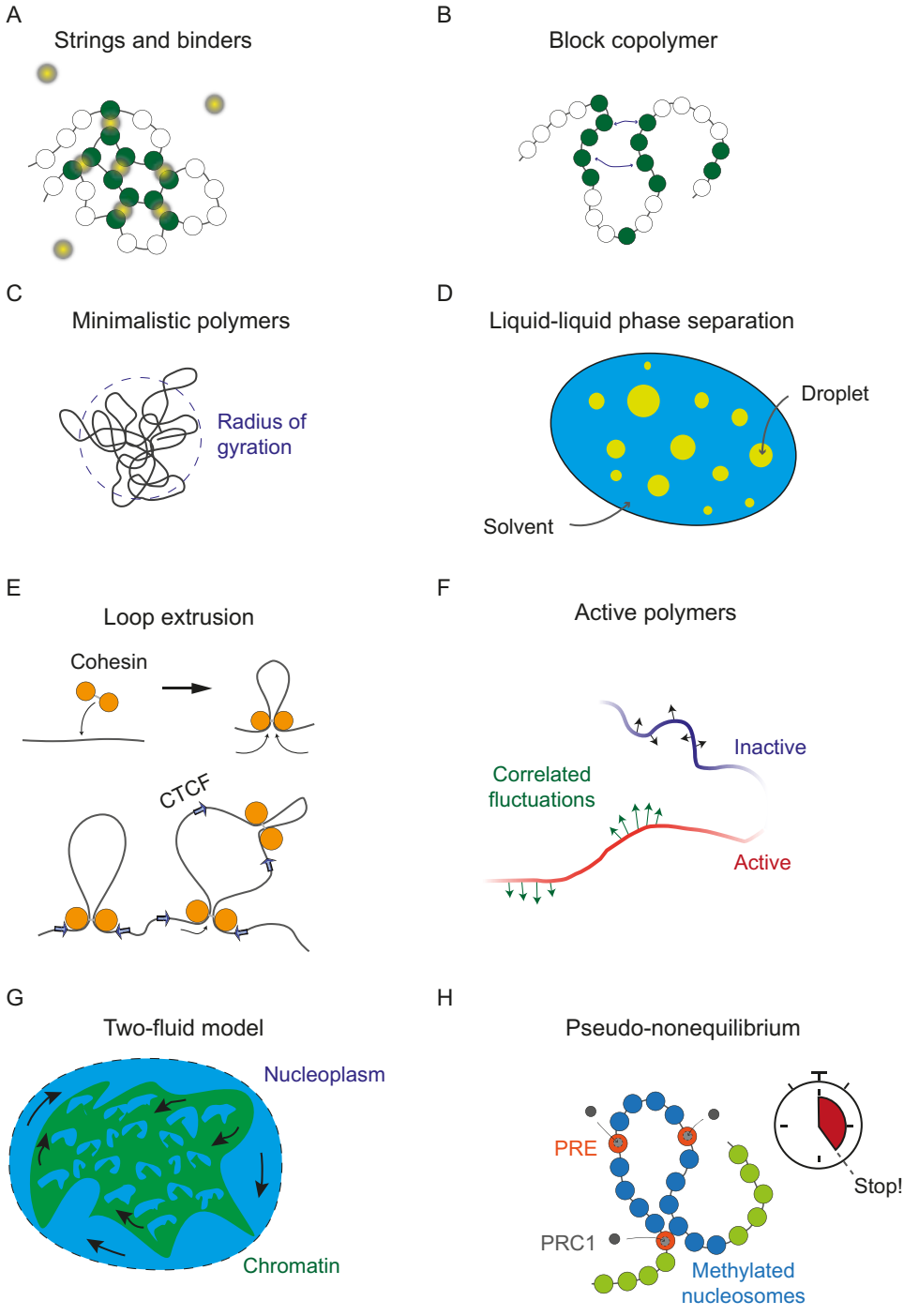

Fig. 5. Computational models of the genome folding. (**A**) Strings-and-binders-switch (SBS) models. Diffusing particles bind to select polymer sites (green) and from bridges. (**B**) Block copolymer models. Identical monomer types attract each other (green), causing the polymer to fold. (**C**) Minimalistic polymers fold due to topological constraints (e.g., self-avoiding polymers or fractal globules). (**D**) Liquid-liquid phase separation models. In such models, protein-protein or protein-chromatin interactions lead to spatial phase separation into liquid-like droplets. Models (A) to (D) assume that the system has reached thermodynamic equilibrium. (**E**) Loop-extrusion model. Cohesin (yellow) associates with chromatin and extrudes chromatin to form a loop. The extrusion stops when the cohesin complex encounters the CTCF protein bound to its recognition sequence (blue arrow). (**F**) "Active" polymers experiencing correlated forces (arrows) along the chromatin. This mimics ATP-dependent processes acting on chromatin, such as transcription. Monomers of "inactive" polymers (blue) experience uncorrelated random (Brownian) motion. (**G**) Two-fluid model. One fluid is compressible and deformable and represents chromatin (green). Like in (F), the chromatin fluid is active. The other fluid represents the nucleoplasm (blue). (**H**) Pseudo-nonequilibrium model. Specific monomers [here, Polycomb response elements (PREs), orange] attract the protein complexes [here, exemplified by the Polycom repressive complex 1 (PRC1), gray]. Stochastic interactions of PRC1 with H3K27 tri-methylated nucleosomes fold the methylated chromatin. After a short time, some process forces PRC1 to dissociate and the simulation stops. Models (E), (F), and (G) belong to the group of nonequilibrium models.

models (Fig. 5B). In one prominent example, the authors reproduce Hi-C maps from *Drosophila* and HeLa cells using a four-state block copolymer representing distinct "epigenetic states" (*101*). Of note, the number of chromatin states in the block copolymer is decided by the modeler. The more states are included in the model, the more parameters the model has available to fit the empirical data. However, including many parameters and making the model more complex carry a substantial risk of overfitting. This may lead to reduced predictive power for biological settings different from those used for parameter optimization. There is no golden standard or consensus on the optimal number of block copolymer states. For example, an influential study used a simple two-state block copolymer model to explain unusual genome architecture with the central position of transcriptionally inactive regions in the rod cells of nocturnal mammals (*102*).

Less widely used are the minimalistic polymer models (Fig. 5C). One of the first groundbreaking models of that kind, mentioned in one of the preceding sections, was that of the fractal (or "crumpled") polymer (*25*). In this model, the chromatin chain is thought to adopt a densely packed, globular conformation constrained by excluded volume interactions. Among other things, the model predicts that the contact probability between two polymer points separated by distance l decays as $1/l$, which is compatible with long-range interactions. Almost two decades after the fractal globule model was proposed, the first measurements of contact frequencies across the human genome using Hi-C concluded that the average contact frequency does decay as predicted by the model (*26*). Apart from predicting contact probabilities, fractal globules represent attractive structures for chromatin folding because they lack knots and have globule-within-globule hierarchies that would facilitate unfolding and refolding, for example, during gene activation, gene repression, or the genome folding into mitotic chromosomes (*92*). Several studies further extended the original fractal polymer framework to better capture the complexity of actual chromatin folding (*95*). Those include a self-avoiding chromatin model under high confinement to explain varying contact probability decay among chromosomes (*103*) and models incorporating various forms of chromatin looping (*104*, *105*).

Our overview of equilibrium models will not be complete without mentioning the approach that treats chromatin segregation as a liquid-liquid phase transition (Fig. 5D). The mechanics of liquid-liquid phase separation depends on the combination of protein-protein and protein-chromatin interactions that form spatially distributed phases, or "droplets," with varying protein densities and composition (*106*, *107*). Undoubtedly, the most cited example of chromatin segregation driven by liquid-liquid phase separation is the nucleolus, the membraneless nuclear organelle, and the primary site for the ribosome subunit assembly (*108*). Liquid-liquid phase separation was also suggested to segregate the centromere-proximal repeat-rich parts of *Drosophila* chromosomes (so-called pericentrometic heterochromatin) from the rest of the genome due to liquid-liquid demixing of the heterochromatin protein 1 (HP1) retained in these regions via interactions with histone H3 methylated at lysine-9 (*109*). Several studies attempted to recapitulate the latter process by numerical modeling. In these models, chromatin, represented as a polymer chain, was surrounded by "HP1 particles" (sometimes, dimers) that had binding affinities to each other and the polymer. By exploring model behavior over the range of HP1 concentrations and affinities to chromatin, it was possible to construct phase diagrams and predict conditions required for liquid-liquid phase separation (*110*–*113*). To what extent the liquid-liquid phase separation is common inside living cells is a subject of debate. We refer the interested reader to the excellent review by McSwiggen and coauthors, who discuss the challenges of distinguishing phase separation from alternative self-organization processes in vivo and provide recommendations for experiments that may settle the issue (*114*).

THE INSIGHTS FROM NONEQUILIBRIUM MODELS

While useful to describe many aspects of genome architecture at the mesoscale, the equilibrium models sweep under the rug the simple truth that living systems are typically far from the thermodynamic equilibrium. Thus, chromatin constantly rearranges and fluctuates not only due to the passive Brownian motion but also via active processes requiring energy, such as chromatin remodeling, transcription, and DNA repair. Tracking of single loci shows a wide variety of anomalous behaviors (*115*–*117*). For example, measuring the mean-squared displacement (MSD) over a time interval t in human retinal pigment epithelial cells indicates that $\mathrm{MSD}(t) = \text{const.} \times t^{0.28}$ (*116*). While this exponent is not universal (*118*), most experiments report deviations from the linear relationship [$\mathrm{MSD}(t) \propto t$] characteristic of standard Brownian motion. In line with these observations, chromatin motion appears to change with ATP concentration, and regions with correlated movement decouple once ATP is depleted (*119*, *120*).

Understanding these processes requires nonequilibrium models of polymer folding and dynamics. The most appreciated group of nonequilibrium models is based on the idea that loop-extruding factors, hypothesized to be cohesins, form progressively larger chromatin loops but stall at TAD boundaries due to interactions with insulator proteins, including CTCF (*85*, *87*, *88*) (Fig. 5E). The models appear to explain the source of chromatin intermixing inside TADs, why chromatin loops do not overlap, and why the TAD borders coincide with convergent CTCF recognition sequences (*121*). Supporting theoretical predictions, chromatin extrusion by cohesin and condensin complexes was demonstrated in vitro (*122*, *123*) and in mouse embryonic stem cells (*86*). Moreover, acute depletion of CTCF or cohesin in human or mouse cells in vitro (*47*, *124*) or in mouse liver cells in vivo (*125*) had a marked effect on the partitioning of their genome into TADs.

Whether cohesin-mediated loop extrusion drives mesoscale genome folding and TAD formation in organisms other than vertebrates remains an open question. For example, in *Drosophila*, CTCF ablation has a limited effect on TAD patterns (*81*, *89*), and the question of whether cohesin complexes have elevated presence at insulator elements is a subject of debate. Thus, the original mapping of cohesin complexes indicated that they preferentially bind transcribed regions and overlap with RNA polymerase II (*126*) with no obvious elevated presence at CTCF binding sites (*127*), which would be expected if chromatin insulator elements impair contacts by stalling loop extruding cohesin complexes. However, a later study challenged these findings suggesting that half of the *Drosophila* CTCF binding sites also bind the cohesin subunits Rad21 (*128*). In line with this claim, *Drosophila* CTCF was shown to interact with Rad21 in vitro (*89*) and co-purify with cohesin subunits from nuclear protein extracts (*82*). However, *Drosophila* insulator elements impair chromatin contacts without forming probabilistic loop-dot contact patterns, which would be expected if they block chromatin contacts generated by loop extrusion (*48*–*50*, *81*). An experiment that assesses the changes in TAD patterns following an acute depletion of cohesin in *Drosophila* cells would be the best way to settle the issue.

Regardless of whether it operates outside the vertebrate lineage, the cohesin-mediated loop extrusion is not responsible for longer-range interaction patterns of A and B compartments (*125*). These seem to emerge from distinct, likely competing, processes. Several studies attempted to develop computer models that combine these processes by mixing active loop extrusion on a short scale and equilibrium binding of pairwise attraction between chromatin segments decorated with histones carrying similar combinations of posttranslational modifications (*129*, *130*). These models reproduce general contact patterns detected by Hi-C and may serve as a suitable testing ground to better understand the effects of knockout experiments that affect only the loop extrusion process.

An entirely different modeling approach exploits the idea that active processes like transcription induce local chromatin motion, which varies as a function of the genomic coordinate (Fig. 5F) (*131*). By combining analytical theory and simulations of a polymer subjected to genomic position-dependent correlated active forces, it is possible to show that a local increase in activity can cause the polymer backbone to bend and expand, while less active segments straighten out and condense. Even modest activity differences appear to drive mesoscale genome folding consistent with the patterns observed by Hi-C.

More abstract nonequilibrium models may be useful to describe coordinated movements of the genome segments discussed at the beginning of this section (*119*, *120*). While this coherence may be interpreted as distant mechanical coupling between loci, the modeling suggests that it may also emerge naturally from polymer folding under nonequilibrium conditions (*132*, *133*). An interesting approach to describe this coordinated chromatin motion is provided by chromatin hydrodynamics (*134*, *135*), which builds on general theories for active matter (*136*). Chromatin hydrodynamics (Fig. 5G) is a two-fluid model with the nucleoplasm playing the role of the solvent (fluid 1) and the chromatin fiber that of a solute (fluid 2). Fluid 2 (chromatin) is highly deformable and compressible and subject to passive thermal fluctuations and active energy-consuming ATP-dependent forces. This model gives rise to complex velocity profiles observed in experiments (*119*) and offers a mechanistic explanation of how long-ranged spatial correlations emerge naturally. Recent use of this framework predicts three types of coordinated phases for chromatin dynamics: disordered and two types of polar order, transverse flows and an oscillatory regime (*137*).

Last, we remark on an emerging "pseudo-nonequilibrium" approach that examines the changes in chromatin folding when introducing specific molecular interactions (Fig. 5H). In contrast to traditional SBS and block copolymer models, a pseudo-nonequilibrium model introduces a "new" interaction to a chromatin fiber that has been in the equilibrium and proceeds with molecular dynamics simulations but stops them after a short time characteristic of a typical binding time of protein(s) under study. In a recent example, such model was developed to study the folding of *Drosophila* genes repressed by the PREs and associated Polycomb repressive complexes (*138*). By scanning a range of binding constants, the study demonstrates that stochastic interactions of PRE-tethered Polycomb repressive complexes with histone H3 tri-methylated at lysine-27 are sufficient to fold the methylated chromatin and thereby translate epigenetic marking of these loci into chromatin folding. In line with Hi-C observations (*48*, *49*), such folding automatically brings PREs in spatial proximity (*138*).

LINKING GENOME ARCHITECTURE TO GENE REGULATION

As we discussed in previous sections, some of the genome folding patterns correlate with high or low transcriptional activity and the expression of corresponding genes. Therefore, it is tempting to speculate that genome folding plays a causative role in controlling transcription and that certain patterns of chromatin folding are either "good" or "bad" for it. In some instances, for example nucleosome placement at specific genomic locations (nucleosome positioning), the connection with transcription initiation is well-documented (*139*, *140*). It is easy to appreciate how the binding of a sequence-specific transcription factor is occluded when its recognition sequence is bound by the histone octamer.

The story becomes more complex when we consider the chromatin folding at the mesoscale. In this case, the folding patterns may reflect the basic dynamics of a polymer in solution and may emerge naturally without the need to evolutionarily select for such behavior. In other words, as long as the probabilistic folding of some sort does not affect transcription too much, it may be tolerated and not selected against. To what extent the partitioning of the genome into TADs is generally important for timely, cell-type–specific gene expression remains a subject of debate.

On the one hand, it has been long known that chromatin insulators are critical to ensure that correct enhancers activate correct genes of *Drosophila* homeotic gene clusters in specific cells (*68*, *70*, *141*). Some of these chromatin insulators, for example, the *Fub* element, form the robust TAD boundary (*79*, *81*). In flies where *Fub* function is abolished by the ablation of the critical effector protein, the two neighboring TADs fuse (*81*), and the homeotic gene located in one of the TADs becomes activated in the wrong part of the fly embryo by the enhancer located in the other TAD (*64*, *70*, *79*). Likewise, the inversions and deletions that remove or reposition the DNA underneath the TAD boundary between mouse *Wnt family member 6* (*Wnt6*), *Indian hedgehog* (*Ihh*), and *paired box 3* (*Pax3*) genes and the *Eph receptor A4* (*Epha4*) gene lead to erroneous activation of the former genes by the *Epha4* enhancers (*142*). In a larger-scale study, CRISPR-Cas9 editing was used to individually delete eight TAD boundaries from the mouse genome (*143*). Seven of the eight deletion mutants had detectable changes in local 3D chromatin architecture, including the merging of TADs and altered contact frequencies within TADs adjacent to the deleted boundary. Five of the eight mutants (63%) displayed increased embryonic lethality or other developmental phenotypes. This suggests that DNA underlying the TAD borders is generally important for proper gene regulation. However, unlike the aforementioned studies where TAD borders concerned were limited to narrow regions of about 2 kb, the TAD borders defined by Rajderkar and coauthors (*143*) were broad regions of 11 to 80 kb, which, in some instances, included multiple transcriptionally active genes and, possibly, their regulatory regions. Therefore, it is hard to exclude that, in this case, some of the changes in gene transcription and developmental phenotypes resulted from the removal of critical enhancer/repressor elements or bringing erroneous enhancers in the proximity of developmental genes located in one of the TADs.

On the other hand, manipulations of the TAD structure within the mouse *sonic hedgehog* (*Shh*) locus had no readily detectable effect on *Shh* expression patterns or levels of Shh expression during development and resulted in no detectable phenotypes (*144*). Even more notable, acute depletion of CTCF or cohesin in human or mouse cells in vitro (*47*, *124*) or in mouse liver cells in vivo (*125*) had a marked effect on the partitioning of the genome into TADs. However, this was

accompanied by modest effects on gene transcription. These changes in transcription of relatively few genes may nevertheless be important at the organismal level. Thus, partial loss of cohesin function that does not alter chromosome segregation causes serious birth defects leading to the Cornelia de Lange syndrome (CdLS) due to improper transcriptional regulation of key developmental genes (*145*, *146*). To what extent transcriptional defects associated with CdLS are mechanistically linked to faults in TAD formation (e.g., due to the impaired chromatin loop extrusion) requires further investigation.

Hi-C comparison of contact patterns in the genomes of wild-type *Drosophila* embryos to those from mutants with disrupted dorsoventral axis showed that widespread differences in gene transcription in the mutants are not paralleled by notable changes in the genome folding, which remain largely the same in the control and mutant embryos (*147*). Likewise, the Hi-C profiling of genomic contacts in a *Drosophila* strain with highly rearranged "balancer" chromosomes revealed many instances of TAD disruptions, which, however, were not predictive of changes in transcription (*148*). In this strain, gene transcription around inversion breakpoints was generally not altered, suggesting that erroneous enhancer-promoter activation or disruption thereof due to TAD defects was a rare event. One caveat of the latter study is that *Drosophila* strains with balancer chromosomes have been deliberately selected for many generations to be viable and fertile. Therefore, we cannot exclude that the strain examined by Ghavi-Helm and coauthors represents a rare exception rather than a general case.

The two opposing views on the importance of the mesoscale genome architecture for gene regulation may converge if the general genome folding patterns play a role only in certain cell types or only under specific environmental conditions. Consistent with this view, the depletion of CTCF or cohesin in mouse cells leads to increased cell-to-cell variability in gene transcription, which is not apparent from bulk population assays (*149*, *150*). Future experiments that combine genetic perturbations with cell-type–specific readouts are required to test this hypothesis.

CONCLUDING REMARKS

Despite the incredible progress of the last decade that transformed our views on many aspects of the eukaryotic genome architecture, more discoveries are awaiting just around the corner. It will be fascinating to learn whether chromatin loop extrusion by cohesin or some other protein complexes is responsible for chromatin intermixing and TAD patterns in animals other than mammals. Equally interesting are the molecular mechanisms by which chromatin insulator elements hinder genomic contacts in species like *Drosophila*. On a different scale of genome folding, we await to fully understand the molecular constraints that prevent chromosome intermixing as well as molecular processes that enable the somatic pairing of homologous chromosomes in some of the insect cells.

Most theoretical models discussed in this review can reproduce genome contact maps derived from the Hi-C assays: SBS, block copolymer, minimalistic polymer, and active polymer models. It has been possible to derive an analytical mapping from a nonequilibrium active polymer model to an effective equilibrium model where the folding is determined by pairwise affinities (*131*). Nevertheless, even models that faithfully reproduce the same Hi-C maps differ widely on other variables, e.g., dynamic quantities of spatial fluctuations of select loci. This argues that the Hi-C contact maps represent but one facet of chromosome 3D organization, which, at best, serves as the minimal requirement for a comprehensive theory of chromatin 3D structure and dynamics.

We foresee that the focus of genome architecture studies will gradually shift from documenting the folding patterns with ever-increasing precision and in a greater number of cell types to investigations of the dynamics with which specific genomic regions alternate between different folding configurations. Here, pathological changes in the CdLS provide an interesting case in point. The CdLS is caused by the partial loss of cohesin function. However, it remains to be seen whether the associated defects in the transcription of developmental genes are due to the changes in the preferred folding patterns or to the overall drop in the frequency with which any two genomic sites (including enhancers and promoters) come in spatial proximity because of the less efficient chromatin loop extrusion. Emerging live imaging techniques, for example, those based on CRISPR-Cas9–mediated locus tagging (*151*), and new nonequilibrium computational models are likely to accelerate the anticipated shift.

REFERENCES AND NOTES

1. K. Luger, A. W. Mader, R. K. Richmond, D. F. Sargent, T. J. Richmond, Crystal structure of the nucleosome core particle at 2.8 A resolution. *Nature* **389**, 251–260 (1997).
2. T. J. Richmond, C. A. Davey, The structure of DNA in the nucleosome core. *Nature* **423**, 145–150 (2003).
3. C. Y. Y. Chong, L. Gan, Are extraordinary nucleosome structures more ordinary than we thought? *Chromosoma* **132**, 139–152 (2023).
4. Z. Y. Tan, S. Cai, A. J. Noble, J. K. Chen, J. Shi, L. Gan, Heterogeneous non-canonical nucleosomes predominate in yeast cells in situ. *eLife* **12**, (2023).
5. S. Baldi, S. Krebs, H. Blum, P. B. Becker, Genome-wide measurement of local nucleosome array regularity and spacing by nanopore sequencing. *Nat. Struct. Mol. Biol.* **25**, 894–901 (2018).
6. B. Lai, W. Gao, K. Cui, W. Xie, Q. Tang, W. Jin, G. Hu, B. Ni, K. Zhao, Principles of nucleosome organization revealed by single-cell micrococcal nuclease sequencing. *Nature* **562**, 281–285 (2018).
7. S. Baldi, P. Korber, P. B. Becker, Beads on a string-nucleosome array arrangements and folding of the chromatin fiber. *Nat. Struct. Mol. Biol.* **27**, 109–118 (2020).
8. S. Eustermann, A. B. Patel, K. P. Hopfner, Y. He, P. Korber, Energy-driven genome regulation by ATP-dependent chromatin remodellers. *Nat. Rev. Mol. Cell Biol.*, (2023).
9. T. Cremer, M. Cremer, Chromosome territories. *Cold Spring Harb. Perspect. Biol.* **2**, a003889 (2010).
10. A. Bolzer, G. Kreth, I. Solovei, D. Koehler, K. Saracoglu, C. Fauth, S. Muller, R. Eils, C. Cremer, M. R. Speicher, T. Cremer, Three-dimensional maps of all chromosomes in human male fibroblast nuclei and prometaphase rosettes. *PLOS Biol.* **3**, e157 (2005).
11. M. Schardin, T. Cremer, H. D. Hager, M. Lang, Specific staining of human chromosomes in Chinese hamster x man hybrid cell lines demonstrates interphase chromosome territories. *Hum. Genet.* **71**, 281–287 (1985).
12. H. Tanabe, S. Muller, M. Neusser, J. von Hase, E. Calcagno, M. Cremer, I. Solovei, C. Cremer, T. Cremer, Evolutionary conservation of chromosome territory arrangements in cell nuclei from higher primates. *Proc. Natl. Acad. Sci. U.S.A.* **99**, 4424–4429 (2002).
13. S. Boyle, S. Gilchrist, J. M. Bridger, N. L. Mahy, J. A. Ellis, W. A. Bickmore, The spatial organization of human chromosomes within the nuclei of normal and emerin-mutant cells. *Hum. Mol. Genet.* **10**, 211–219 (2001).
14. M. Cremer, K. Kupper, B. Wagler, L. Wizelman, J. von Hase, Y. Weiland, L. Kreja, J. Diebold, M. R. Speicher, T. Cremer, Inheritance of gene density-related higher order chromatin arrangements in normal and tumor cell nuclei. *J. Cell Biol.* **162**, 809–820 (2003).
15. J. A. Croft, J. M. Bridger, S. Boyle, P. Perry, P. Teague, W. A. Bickmore, Differences in the localization and morphology of chromosomes in the human nucleus. *J. Cell Biol.* **145**, 1119–1131 (1999).
16. K. Kupper, A. Kolbl, D. Biener, S. Dittrich, J. von Hase, T. Thormeyer, H. Fiegler, N. P. Carter, M. R. Speicher, T. Cremer, M. Cremer, Radial chromatin positioning is shaped by local gene density, not by gene expression. *Chromosoma* **116**, 285–306 (2007).
17. A. E. Murmann, J. Gao, M. Encinosa, M. Gautier, M. E. Peter, R. Eils, P. Lichter, J. D. Rowley, Local gene density predicts the spatial position of genetic loci in the interphase nucleus. *Exp. Cell Res.* **311**, 14–26 (2005).
18. L. Brianna Caddle, J. L. Grant, J. Szatkiewicz, J. van Hase, B. J. Shirley, J. Bewersdorf, C. Cremer, A. Arneodo, A. Khalil, K. D. Mills, Chromosome neighborhood composition determines translocation outcomes after exposure to high-dose radiation in primary cells. *Chromosome Res.* **15**, 1061–1073 (2007).

19. L. A. Parada, P. G. McQueen, P. J. Munson, T. Misteli, Conservation of relative chromosome positioning in normal and cancer cells. *Curr. Biol.* **12**, 1692–1697 (2002).
20. J. J. Roix, P. G. McQueen, P. J. Munson, L. A. Parada, T. Misteli, Spatial proximity of translocation-prone gene loci in human lymphomas. *Nat. Genet.* **34**, 287–291 (2003).
21. C. R. Keenan, M. J. Mlodzianoski, H. D. Coughlan, N. G. Bediaga, G. Naselli, E. C. Lucas, Q. Wang, C. A. de Graaf, D. J. Hilton, L. C. Harrison, G. K. Smyth, K. L. Rogers, T. Boudier, R. S. Allan, T. M. Johanson, Chromosomes distribute randomly to, but not within, human neutrophil nuclear lobes. *iScience* **24**, 102161 (2021).
22. J. D. Halverson, J. Smrek, K. Kremer, A. Y. Grosberg, From a melt of rings to chromosome territories: The role of topological constraints in genome folding. *Rep. Prog. Phys.* **77**, 022601 (2014).
23. M. D. Rubinstein, R. H. Colby, *Polymer Physics* (Oxford Univ. Press, 2003).
24. A. Rosa, R. Everaers, Structure and dynamics of interphase chromosomes. *PLOS Comput. Biol.* **4**, e1000153 (2008).
25. A. Grosberg, Y. Rabin, S. Havlin, A. Neer, Crumpled globule model of the three-dimensional structure of DNA. *Europhys. Lett.* **23**, 373–378 (1993).
26. E. Lieberman-Aiden, N. L. van Berkum, L. Williams, M. Imakaev, T. Ragoczy, A. Telling, I. Amit, B. R. Lajoie, P. J. Sabo, M. O. Dorschner, R. Sandstrom, B. Bernstein, M. A. Bender, M. Groudine, A. Gnirke, J. Stamatoyannopoulos, L. A. Mirny, E. S. Lander, J. Dekker, Comprehensive mapping of long-range interactions reveals folding principles of the human genome. *Science* **326**, 289–293 (2009).
27. E. F. Joyce, J. Erceg, C. T. Wu, Pairing and anti-pairing: A balancing act in the diploid genome. *Curr. Opin. Genet. Dev.* **37**, 119–128 (2016).
28. M. B. T. Child, J. R. Bateman, A. Jahangiri, A. Reimer, N. C. Lammers, N. Sabouni, D. Villamarin, G. C. McKenzie-Smith, J. E. Johnson, D. Jost, H. G. Garcia, Live imaging and biophysical modeling support a button-based mechanism of somatic homolog pairing in Drosophila. *eLife* **10**, (2021).
29. W. F. Marshall, J. C. Fung, Homologous chromosome recognition via nonspecific interactions. bioRxiv (2023).
30. M. Eltsov, K. M. Maclellan, K. Maeshima, A. S. Frangakis, J. Dubochet, Analysis of cryo-electron microscopy images does not support the existence of 30-nm chromatin fibers in mitotic chromosomes in situ. *Proc. Natl. Acad. Sci. U.S.A.* **105**, 19732–19737 (2008).
31. E. Fussner, M. Strauss, U. Djuric, R. Li, K. Ahmed, M. Hart, J. Ellis, D. P. Bazett-Jones, Open and closed domains in the mouse genome are configured as 10-nm chromatin fibres. *EMBO Rep.* **13**, 992–996 (2012).
32. H. D. Ou, S. Phan, T. J. Deerinck, A. Thor, M. H. Ellisman, C. C. O'Shea, ChromEMT: Visualizing 3D chromatin structure and compaction in interphase and mitotic cells. *Science* **357**, (2017).
33. M. E. Pownall, L. Miao, C. E. Vejnar, O. M'Saad, A. Sherrard, M. A. Frederick, M. D. J. Benitez, C. W. Boswell, K. S. Zaret, J. Bewersdorf, A. J. Giraldez, Chromatin expansion microscopy reveals nanoscale organization of transcription and chromatin. *Science* **381**, 92–100 (2023).
34. J. Dekker, K. Rippe, M. Dekker, N. Kleckner, Capturing chromosome conformation. *Science* **295**, 1306–1311 (2002).
35. I. Jerkovic, G. Cavalli, Understanding 3D genome organization by multidisciplinary methods. *Nat. Rev. Mol. Cell Biol.* **22**, 511–528 (2021).
36. S. Sati, G. Cavalli, Chromosome conformation capture technologies and their impact in understanding genome function. *Chromosoma* **126**, 33–44 (2017).
37. T. Sexton, E. Yaffe, E. Kenigsberg, F. Bantignies, B. Leblanc, M. Hoichman, H. Parrinello, A. Tanay, G. Cavalli, Three-dimensional folding and functional organization principles of the Drosophila genome. *Cell* **148**, 458–472 (2012).
38. J. R. Dixon, S. Selvaraj, F. Yue, A. Kim, Y. Li, Y. Shen, M. Hu, J. S. Liu, B. Ren, Topological domains in mammalian genomes identified by analysis of chromatin interactions. *Nature* **485**, 376–380 (2012).
39. E. de Wit, TADs as the Caller Calls Them. *J. Mol. Biol.* **432**, 638–642 (2020).
40. E. Sefer, A comparison of topologically associating domain callers over mammals at high resolution. *BMC Bioinformatics* **23**, 127 (2022).
41. B. Bonev, N. Mendelson Cohen, Q. Szabo, L. Fritsch, G. L. Papadopoulos, Y. Lubling, X. Xu, X. Lv, J. P. Hugnot, A. Tanay, G. Cavalli, Multiscale 3D Genome Rewiring during Mouse Neural Development. *Cell* **171**, 557–572.e24 (2017).
42. O. Joshi, S. Y. Wang, T. Kuznetsova, Y. Atlasi, T. Peng, P. J. Fabre, E. Habibi, J. Shaik, S. Saeed, L. Handoko, T. Richmond, M. Spivakov, D. Burgess, H. G. Stunnenberg, Dynamic reorganization of extremely long-range promoter-promoter interactions between two states of pluripotency. *Cell Stem Cell* **17**, 748–757 (2015).
43. K. Kraft, K. E. Yost, S. E. Murphy, A. Magg, Y. Long, M. R. Corces, J. M. Granja, L. Wittler, S. Mundlos, T. R. Cech, A. N. Boettiger, H. Y. Chang, Polycomb-mediated genome architecture enables long-range spreading of H3K27 methylation. *Proc. Natl. Acad. Sci. U.S.A.* **119**, e2201883119 (2022).
44. J. D. P. Rhodes, A. Feldmann, B. Hernandez-Rodriguez, N. Diaz, J. M. Brown, N. A. Fursova, N. P. Blackledge, P. Prathapan, P. Dobrinic, M. K. Huseyin, A. Szczurek, K. Kruse, K. A. Nasmyth, V. J. Buckle, J. M. Vaquerizas, R. J. Klose, Cohesin disrupts polycomb-dependent chromosome interactions in embryonic stem cells. *Cell Rep.* **30**, 820–835.e10 (2020).
45. B. Tolhuis, M. Blom, R. M. Kerkhoven, L. Pagie, H. Teunissen, M. Nieuwland, M. Simonis, W. de Laat, M. van Lohuizen, B. van Steensel, Interactions among Polycomb domains are guided by chromosome architecture. *PLOS Genet.* **7**, e1001343 (2011).
46. S. S. Rao, M. H. Huntley, N. C. Durand, E. K. Stamenova, I. D. Bochkov, J. T. Robinson, A. L. Sanborn, I. Machol, A. D. Omer, E. S. Lander, E. L. Aiden, A 3D map of the human genome at kilobase resolution reveals principles of chromatin looping. *Cell* **159**, 1665–1680 (2014).
47. S. S. P. Rao, S. C. Huang, B. G. S. Hilaire, J. M. Engreitz, E. M. Perez, K. R. Kieffer-Kwon, A. L. Sanborn, S. E. Johnstone, G. D. Bascom, I. D. Bochkov, X. Huang, M. S. Shamim, J. Shin, D. Turner, Z. Ye, A. D. Omer, J. T. Robinson, T. Schlick, B. E. Bernstein, R. Casellas, E. S. Lander, E. L. Aiden, Cohesin loss eliminates all loop domains. *Cell* **171**, 305–320.e24 (2017).
48. K. P. Eagen, E. L. Aiden, R. D. Kornberg, Polycomb-mediated chromatin loops revealed by a subkilobase-resolution chromatin interaction map. *Proc. Natl. Acad. Sci. U.S.A.* **114**, 8764–8769 (2017).
49. Y. Ogiyama, B. Schuettengruber, G. L. Papadopoulos, J. M. Chang, G. Cavalli, Polycomb-dependent chromatin looping contributes to gene silencing during drosophila development. *Mol. Cell* **71**, 73–88.e5 (2018).
50. P. J. Batut, X. Y. Bing, Z. Sisco, J. Raimundo, M. Levo, M. S. Levine, Genome organization controls transcriptional dynamics during development. *Science* **375**, 566–570 (2022).
51. X. Li, X. Tang, X. Bing, C. Catalano, T. Li, G. Dolsten, C. Wu, M. Levine, GAGA-associated factor fosters loop formation in the Drosophila genome. *Mol. Cell* **83**, 1519–1526.e4 (2023).
52. R. A. Beagrie, A. Scialdone, M. Schueler, D. C. Kraemer, M. Chotalia, S. Q. Xie, M. Barbieri, I. de Santiago, L. M. Lavitas, M. R. Branco, J. Fraser, J. Dostie, L. Game, N. Dillon, P. A. Edwards, M. Nicodemi, A. Pombo, Complex multi-enhancer contacts captured by genome architecture mapping. *Nature* **543**, 519–524 (2017).
53. S. A. Quinodoz, N. Ollikainen, B. Tabak, A. Palla, J. M. Schmidt, E. Detmar, M. M. Lai, A. A. Shishkin, P. Bhat, Y. Takei, V. Trinh, E. Aznauryan, P. Russell, C. Cheng, M. Jovanovic, A. Chow, L. Cai, P. McDonel, M. Garber, M. Guttman, Higher-order inter-chromosomal hubs shape 3D genome organization in the nucleus. *Cell* **174**, 744–757.e24 (2018).
54. S. A. Quinodoz, J. W. Jachowicz, P. Bhat, N. Ollikainen, A. K. Banerjee, I. N. Goronzy, M. R. Blanco, P. Chovanec, A. Chow, Y. Markaki, J. Thai, K. Plath, M. Guttman, RNA promotes the formation of spatial compartments in the nucleus. *Cell* **184**, 5775–5790.e30 (2021).
55. D. L. J. Lafontaine, J. A. Riback, R. Bascetin, C. P. Brangwynne, The nucleolus as a multiphase liquid condensate. *Nat. Rev. Mol. Cell Biol.* **22**, 165–182 (2021).
56. D. L. Spector, A. I. Lamond, Nuclear speckles. *Cold Spring Harb. Perspect. Biol.* **3**, a000646 (2011).
57. Y. M. Sigal, R. Zhou, X. Zhuang, Visualizing and discovering cellular structures with super-resolution microscopy. *Science* **361**, 880–887 (2018).
58. A. Boettiger, S. Murphy, Advances in chromatin imaging at kilobase-scale resolution. *Trends Genet.* **36**, 273–287 (2020).
59. B. Bintu, L. J. Mateo, J. H. Su, N. A. Sinnott-Armstrong, M. Parker, S. Kinrot, K. Yamaya, A. N. Boettiger, X. Zhuang, Super-resolution chromatin tracing reveals domains and cooperative interactions in single cells. *Science* **362**, (2018).
60. Q. Szabo, A. Donjon, I. Jerkovic, G. L. Papadopoulos, T. Cheutin, B. Bonev, E. P. Nora, B. G. Bruneau, F. Bantignies, G. Cavalli, Regulation of single-cell genome organization into TADs and chromatin nanodomains. *Nat. Genet.* **52**, 1151–1157 (2020).
61. D. I. Cattoni, A. M. Cardozo Gizzi, M. Georgieva, M. Di Stefano, A. Valeri, D. Chamousset, C. Houbron, S. Dejardin, J. B. Fiche, I. Gonzalez, J. M. Chang, T. Sexton, M. A. Marti-Renom, F. Bantignies, G. Cavalli, M. Nollmann, Single-cell absolute contact probability detection reveals chromosomes are organized by multiple low-frequency yet specific interactions. *Nat. Commun.* **8**, 1753 (2017).
62. E. H. Finn, G. Pegoraro, H. B. Brandao, A. L. Valton, M. E. Oomen, J. Dekker, L. Mirny, T. Misteli, Extensive heterogeneity and intrinsic variation in spatial genome organization. *Cell* **176**, 1502–1515.e10 (2019).
63. A. M. Cardozo Gizzi, D. I. Cattoni, J. B. Fiche, S. M. Espinola, J. Gurgo, O. Messina, C. Houbron, Y. Ogiyama, G. L. Papadopoulos, G. Cavalli, M. Lagha, M. Nollmann, Microscopy-based chromosome conformation capture enables simultaneous visualization of genome organization and transcription in intact organisms. *Mol. Cell* **74**, 212–222.e5 (2019).
64. L. J. Mateo, S. E. Murphy, A. Hafner, I. S. Cinquini, C. A. Walker, A. N. Boettiger, Visualizing DNA folding and RNA in embryos at single-cell resolution. *Nature* **568**, 49–54 (2019).
65. P. K. Geyer, V. G. Corces, DNA position-specific repression of transcription by a Drosophila zinc finger protein. *Genes Dev.* **6**, 1865–1873 (1992).
66. C. Holdridge, D. Dorsett, Repression of hsp70 heat shock gene transcription by the suppressor of hairy-wing protein of *Drosophila melanogaster*. *Mol. Cell. Biol.* **11**, 1894–1900 (1991).
67. A. Udvardy, E. Maine, P. Schedl, The 87A7 chromomere. Identification of novel chromatin structures flanking the heat shock locus that may define the boundaries of higher order domains. *J. Mol. Biol.* **185**, 341–358 (1985).

68. S. Barges, J. Mihaly, M. Galloni, K. Hagstrom, M. Muller, G. Shanower, P. Schedl, H. Gyurkovics, F. Karch, The Fab-8 boundary defines the distal limit of the bithorax complex iab-7 domain and insulates iab-7 from initiation elements and a PRE in the adjacent iab-8 domain. *Development* **127**, 779–790 (2000).
69. A. C. Bell, G. Felsenfeld, Methylation of a CTCF-dependent boundary controls imprinted expression of the Igf2 gene. *Nature* **405**, 482–485 (2000).
70. W. Bender, M. Lucas, The border between the ultrabithorax and abdominal-A regulatory domains in the Drosophila bithorax complex. *Genetics* **193**, 1135–1147 (2013).
71. M. Fujioka, X. Wu, J. B. Jaynes, A chromatin insulator mediates transgene homing and very long-range enhancer-promoter communication. *Development* **136**, 3077–3087 (2009).
72. A. T. Hark, C. J. Schoenherr, D. J. Katz, R. S. Ingram, J. M. Levorse, S. M. Tilghman, CTCF mediates methylation-sensitive enhancer-blocking activity at the H19/Igf2 locus. *Nature* **405**, 486–489 (2000).
73. F. Karch, M. Galloni, L. Sipos, J. Gausz, H. Gyurkovics, P. Schedl, Mcp and Fab-7: Molecular analysis of putative boundaries of cis-regulatory domains in the bithorax complex of *Drosophila melanogaster*. *Nucleic Acids Res.* **22**, 3138–3146 (1994).
74. A. Sparago, F. Cerrato, M. Vernucci, G. B. Ferrero, M. C. Silengo, A. Riccio, Microdeletions in the human H19 DMR result in loss of IGF2 imprinting and Beckwith-Wiedemann syndrome. *Nat. Genet.* **36**, 958–960 (2004).
75. Y. B. Schwartz, G. Cavalli, Three-dimensional genome organization and function in drosophila. *Genetics* **205**, 5–24 (2017).
76. H. Yao, K. Brick, Y. Evrard, T. Xiao, R. D. Camerini-Otero, G. Felsenfeld, Mediation of CTCF transcriptional insulation by DEAD-box RNA-binding protein p68 and steroid receptor RNA activator SRA. *Genes Dev.* **24**, 2543–2555 (2010).
77. H. Ortabozkoyun, P. Y. Huang, H. Cho, V. Narendra, G. LeRoy, E. Gonzalez-Buendia, J. A. Skok, A. Tsirigos, E. O. Mazzoni, D. Reinberg, CRISPR and biochemical screens identify MAZ as a cofactor in CTCF-mediated insulation at Hox clusters. *Nat. Genet.* **54**, 202–212 (2022).
78. T. Xiao, X. Li, G. Felsenfeld, The Myc-associated zinc finger protein (MAZ) works together with CTCF to control cohesin positioning and genome organization. *Proc. Natl. Acad. Sci. U.S.A.* **118**, e2023127118 (2021).
79. M. Savitsky, M. Kim, O. Kravchuk, Y. B. Schwartz, Distinct roles of chromatin insulator proteins in control of the drosophila bithorax complex. *Genetics* **202**, 601–617 (2016).
80. Y. B. Schwartz, D. Linder-Basso, P. V. Kharchenko, M. Y. Tolstorukov, M. Kim, H. B. Li, A. A. Gorchakov, A. Minoda, G. Shanower, A. A. Alekseyenko, N. C. Riddle, Y. L. Jung, T. Gu, A. Plachetka, S. C. Elgin, M. I. Kuroda, P. J. Park, M. Savitsky, G. H. Karpen, V. Pirrotta, Nature and function of insulator protein binding sites in the Drosophila genome. *Genome Res.* **22**, 2188–2198 (2012).
81. T. G. Kahn, M. Savitsky, C. Kuong, C. Jacquier, G. Cavalli, J. M. Chang, Y. B. Schwartz, Topological screen identifies hundreds of Cp190- and CTCF-dependent Drosophila chromatin insulator elements. *Sci. Adv.* **9**, eade0090 (2023).
82. A. Kaushal, J. Dorier, B. Wang, G. Mohana, M. Taschner, P. Cousin, P. Waridel, C. Iseli, A. Semenova, S. Restrepo, N. Guex, E. L. Aiden, M. C. Gambetta, Essential role of Cp190 in physical and regulatory boundary formation. *Sci. Adv.* **8**, eabl8834 (2022).
83. C. Barrington, D. Georgopoulou, D. Pezic, W. Varsally, J. Herrero, S. Hadjur, Enhancer accessibility and CTCF occupancy underlie asymmetric TAD architecture and cell type specific genome topology. *Nat. Commun.* **10**, 2908 (2019).
84. L. Vian, A. Pekowska, S. S. P. Rao, K. R. Kieffer-Kwon, S. Jung, L. Baranello, S. C. Huang, L. El Khattabi, M. Dose, N. Pruett, A. L. Sanborn, A. Canela, Y. Maman, A. Oksanen, W. Resch, X. Li, B. Lee, A. L. Kovalchuk, Z. Tang, S. Nelson, M. Di Pierro, R. R. Cheng, I. Machol, B. G. St Hilaire, N. C. Durand, M. S. Shamim, E. K. Stamenova, J. N. Onuchic, Y. Ruan, A. Nussenzweig, D. Levens, E. L. Aiden, R. Casellas, The energetics and physiological impact of cohesin extrusion. *Cell* **173**, 1165–1178.e20 (2018).
85. G. Fudenberg, M. Imakaev, C. Lu, A. Goloborodko, N. Abdennur, L. A. Mirny, Formation of chromosomal domains by loop extrusion. *Cell Rep.* **15**, 2038–2049 (2016).
86. M. Gabriele, H. B. Brandao, S. Grosse-Holz, A. Jha, G. M. Dailey, C. Cattoglio, T. S. Hsieh, L. Mirny, C. Zechner, A. S. Hansen, Dynamics of CTCF- and cohesin-mediated chromatin looping revealed by live-cell imaging. *Science* **376**, 496–501 (2022).
87. A. Goloborodko, J. F. Marko, L. A. Mirny, Chromosome compaction by active loop extrusion. *Biophys. J.* **110**, 2162–2168 (2016).
88. A. L. Sanborn, S. S. Rao, S. C. Huang, N. C. Durand, M. H. Huntley, A. I. Jewett, I. D. Bochkov, D. Chinnappan, A. Cutkosky, J. Li, K. P. Geeting, A. Gnirke, A. Melnikov, D. McKenna, E. K. Stamenova, E. S. Lander, E. L. Aiden, Chromatin extrusion explains key features of loop and domain formation in wild-type and engineered genomes. *Proc. Natl. Acad. Sci. U.S.A.* **112**, E6456–E6465 (2015).
89. A. Kaushal, G. Mohana, J. Dorier, I. Ozdemir, A. Omer, P. Cousin, A. Semenova, M. Taschner, O. Dergai, F. Marzetta, C. Iseli, Y. Eliaz, D. Weisz, M. S. Shamim, N. Guex, E. Lieberman Aiden, M. C. Gambetta, CTCF loss has limited effects on global genome architecture in Drosophila despite critical regulatory functions. *Nat. Commun.* **12**, 1011 (2021).
90. G. Mohana, J. Dorier, X. Li, M. Mouginot, R. C. Smith, H. Malek, M. Leleu, D. Rodriguez, J. Khadka, P. Rosa, P. Cousin, C. Iseli, S. Restrepo, N. Guex, B. D. McCabe, A. Jankowski, M. S. Levine, M. C. Gambetta, Chromosome-level organization of the regulatory genome in the Drosophila nervous system. *Cell* **186**, 3826–3844.e26 (2023).
91. B. Schuettengruber, H. M. Bourbon, L. Di Croce, G. Cavalli, Genome regulation by polycomb and trithorax: 70 years and counting. *Cell* **171**, 34–57 (2017).
92. L. A. Mirny, The fractal globule as a model of chromatin architecture in the cell. *Chromosome Res.* **19**, 37–51 (2011).
93. A. M. Chiariello, S. Bianco, A. Esposito, L. Fiorillo, M. Conte, E. Irani, F. Musella, A. Abraham, A. Prisco, M. Nicodemi, Physical mechanisms of chromatin spatial organization. *FEBS J.* **289**, 1180–1190 (2022).
94. D. Jost, Polymer modeling of 3D epigenome folding: Application to drosophila. *Methods Mol. Biol.* **2301**, 293–305 (2022).
95. J. Liang, A. Perez-Rathke, Minimalistic 3D chromatin models: Sparse interactions in single cells drive the chromatin fold and form many-body units. *Curr. Opin. Struct. Biol.* **71**, 200–214 (2021).
96. M. Barbieri, M. Chotalia, J. Fraser, L. M. Lavitas, J. Dostie, A. Pombo, M. Nicodemi, Complexity of chromatin folding is captured by the strings and binders switch model. *Proc. Natl. Acad. Sci. U.S.A.* **109**, 16173–16178 (2012).
97. A. Buckle, C. A. Brackley, S. Boyle, D. Marenduzzo, N. Gilbert, Polymer simulations of heteromorphic chromatin predict the 3d folding of complex genomic loci. *Mol. Cell* **72**, 786–797.e11 (2018).
98. C. Annunziatella, A. M. Chiariello, S. Bianco, M. Nicodemi, Polymer models of the hierarchical folding of the Hox-B chromosomal locus. *Phys. Rev. E.* **94**, 042402 (2016).
99. S. Bianco, D. G. Lupianez, A. M. Chiariello, C. Annunziatella, K. Kraft, R. Schopflin, L. Wittler, G. Andrey, M. Vingron, A. Pombo, S. Mundlos, M. Nicodemi, Polymer physics predicts the effects of structural variants on chromatin architecture. *Nat. Genet.* **50**, 662–667 (2018).
100. C. A. Brackley, N. Gilbert, D. Michieletto, A. Papantonis, M. C. F. Pereira, P. R. Cook, D. Marenduzzo, Complex small-world regulatory networks emerge from the 3D organisation of the human genome. *Nat. Commun.* **12**, 5756 (2021).
101. D. Jost, P. Carrivain, G. Cavalli, C. Vaillant, Modeling epigenome folding: Formation and dynamics of topologically associated chromatin domains. *Nucleic Acids Res.* **42**, 9553–9561 (2014).
102. M. Falk, Y. Feodorova, N. Naumova, M. Imakaev, B. R. Lajoie, H. Leonhardt, B. Joffe, J. Dekker, G. Fudenberg, I. Solovei, L. A. Mirny, Heterochromatin drives compartmentalization of inverted and conventional nuclei. *Nature* **570**, 395–399 (2019).
103. G. Gursoy, Y. Xu, A. L. Kenter, J. Liang, Spatial confinement is a major determinant of the folding landscape of human chromosomes. *Nucleic Acids Res.* **42**, 8223–8230 (2014).
104. M. Bohn, D. W. Heermann, R. van Driel, Random loop model for long polymers. *Phys. Rev. E Stat. Nonlin. Soft Matter Phys.* **76**, 051805 (2007).
105. O. Shukron, D. Holcman, Transient chromatin properties revealed by polymer models and stochastic simulations constructed from Chromosomal Capture data. *PLOS Comput. Biol.* **13**, e1005469 (2017).
106. F. Erdel, Phase transitions in heterochromatin organization. *Curr. Opin. Struct. Biol.* **80**, 102597 (2023).
107. K. Rippe, Liquid-Liquid Phase Separation in Chromatin. *Cold Spring Harb. Perspect. Biol.* **14**, a040683 (2022).
108. C. P. Brangwynne, T. J. Mitchison, A. A. Hyman, Active liquid-like behavior of nucleoli determines their size and shape in Xenopus laevis oocytes. *Proc. Natl. Acad. Sci. U.S.A.* **108**, 4334–4339 (2011).
109. A. R. Strom, A. V. Emelyanov, M. Mir, D. V. Fyodorov, X. Darzacq, G. H. Karpen, Phase separation drives heterochromatin domain formation. *Nature* **547**, 241–245 (2017).
110. M. Ancona, C. A. Brackley, Simulating the chromatin-mediated phase separation of model proteins with multiple domains. *Biophys. J.* **121**, 2600–2612 (2022).
111. R. Laghmach, M. Di Pierro, D. A. Potoyan, The interplay of chromatin phase separation and lamina interactions in nuclear organization. *Biophys. J.* **120**, 5005–5017 (2021).
112. A. P. Latham, B. Zhang, On the stability and layered organization of protein-DNA condensates. *Biophys. J.* **121**, 1727–1737 (2022).
113. M. M. C. Tortora, L. D. Brennan, G. Karpen, D. Jost, HP1-driven phase separation recapitulates the thermodynamics and kinetics of heterochromatin condensate formation. *Proc. Natl. Acad. Sci. U.S.A.* **120**, e2211855120 (2023).
114. D. T. McSwiggen, M. Mir, X. Darzacq, R. Tjian, Evaluating phase separation in live cells: Diagnosis, caveats, and functional consequences. *Genes Dev.* **33**, 1619–1634 (2019).
115. I. Bronshtein, E. Kepten, I. Kanter, S. Berezin, M. Lindner, A. B. Redwood, S. Mai, S. Gonzalo, R. Foisner, Y. Shav-Tal, Y. Garini, Loss of lamin A function increases chromatin dynamics in the nuclear interior. *Nat. Commun.* **6**, 8044 (2015).
116. R. Nagashima, K. Hibino, S. S. Ashwin, M. Babokhov, S. Fujishiro, R. Imai, T. Nozaki, S. Tamura, T. Tani, H. Kimura, M. Shribak, M. T. Kanemaki, M. Sasai, K. Maeshima, Single nucleosome imaging reveals loose genome chromatin networks via active RNA polymerase II. *J. Cell Biol.* **218**, 1511–1530 (2019).
117. T. Nozaki, R. Imai, M. Tanbo, R. Nagashima, S. Tamura, T. Tani, Y. Joti, M. Tomita, K. Hibino, M. T. Kanemaki, K. S. Wendt, Y. Okada, T. Nagai, K. Maeshima, Dynamic organization of chromatin domains revealed by super-resolution live-cell imaging. *Mol. Cell* **67**, 282–293. e7 (2017).

118. Y. Kim, L. Lizana, J. H. Jeon, Fractal and knot-free chromosomes facilitate nucleoplasmic transport. *Phys. Rev. Lett.* **128**, 038101 (2022).
119. D. Saintillan, M. J. Shelley, A. Zidovska, Extensile motor activity drives coherent motions in a model of interphase chromatin. *Proc. Natl. Acad. Sci. U.S.A.* **115**, 11442–11447 (2018).
120. A. Zidovska, D. A. Weitz, T. J. Mitchison, Micron-scale coherence in interphase chromatin dynamics. *Proc. Natl. Acad. Sci. U.S.A.* **110**, 15555–15560 (2013).
121. E. J. Banigan, L. A. Mirny, Loop extrusion: Theory meets single-molecule experiments. *Curr. Opin. Cell Biol.* **64**, 124–138 (2020).
122. M. Ganji, I. A. Shaltiel, S. Bisht, E. Kim, A. Kalichava, C. H. Haering, C. Dekker, Real-time imaging of DNA loop extrusion by condensin. *Science* **360**, 102–105 (2018).
123. Y. Kim, Z. Shi, H. Zhang, I. J. Finkelstein, H. Yu, Human cohesin compacts DNA by loop extrusion. *Science* **366**, 1345–1349 (2019).
124. E. P. Nora, A. Goloborodko, A. L. Valton, J. H. Gibcus, A. Uebersohn, N. Abdennur, J. Dekker, L. A. Mirny, B. G. Bruneau, Targeted degradation of CTCF decouples local insulation of chromosome domains from genomic compartmentalization. *Cell* **169**, 930–944.e22 (2017).
125. W. Schwarzer, N. Abdennur, A. Goloborodko, A. Pekowska, G. Fudenberg, Y. Loe-Mie, N. A. Fonseca, W. Huber, C. H. Haering, L. Mirny, F. Spitz, Two independent modes of chromatin organization revealed by cohesin removal. *Nature* **551**, 51–56 (2017).
126. Z. Misulovin, Y. B. Schwartz, X. Y. Li, T. G. Kahn, M. Gause, S. MacArthur, J. C. Fay, M. B. Eisen, V. Pirrotta, M. D. Biggin, D. Dorsett, Association of cohesin and Nipped-B with transcriptionally active regions of the *Drosophila melanogaster* genome. *Chromosoma* **117**, 89–102 (2008).
127. M. Bartkuhn, T. Straub, M. Herold, M. Herrmann, C. Rathke, H. Saumweber, G. D. Gilfillan, P. B. Becker, R. Renkawitz, Active promoters and insulators are marked by the centrosomal protein 190. *EMBO J.* **28**, 877–888 (2009).
128. K. Van Bortle, M. H. Nichols, L. Li, C. T. Ong, N. Takenaka, Z. S. Qin, V. G. Corces, Insulator function and topological domain border strength scale with architectural protein occupancy. *Genome Biol.* **15**, R82 (2014).
129. M. Conte, E. Irani, A. M. Chiariello, A. Abraham, S. Bianco, A. Esposito, M. Nicodemi, Loop-extrusion and polymer phase-separation can co-exist at the single-molecule level to shape chromatin folding. *Nat. Commun.* **13**, 4070 (2022).
130. J. Nuebler, G. Fudenberg, M. Imakaev, N. Abdennur, L. A. Mirny, Chromatin organization by an interplay of loop extrusion and compartmental segregation. *Proc. Natl. Acad. Sci. U.S.A.* **115**, E6697–E6706 (2018).
131. A. Goychuk, D. Kannan, A. K. Chakraborty, M. Kardar, Polymer folding through active processes recreates features of genome organization. *Proc. Natl. Acad. Sci. U.S.A.* **120**, e2221726120 (2023).
132. M. Di Pierro, D. A. Potoyan, P. G. Wolynes, J. N. Onuchic, Anomalous diffusion, spatial coherence, and viscoelasticity from the energy landscape of human chromosomes. *Proc. Natl. Acad. Sci. U.S.A.* **115**, 7753–7758 (2018).
133. S. Put, T. Sakaue, C. Vanderzande, Active dynamics and spatially coherent motion in chromosomes subject to enzymatic force dipoles. *Phys. Rev. E.* **99**, 032421 (2019).
134. R. Bruinsma, A. Y. Grosberg, Y. Rabin, A. Zidovska, Chromatin hydrodynamics. *Biophys. J.* **106**, 1871–1881 (2014).
135. I. Eshghi, A. Zidovska, A. Y. Grosberg, Symmetry-based classification of forces driving chromatin dynamics. *Soft Matter* **18**, 8134–8146 (2022).
136. F. Julicher, S. W. Grill, G. Salbreux, Hydrodynamic theory of active matter. *Rep. Prog. Phys.* **81**, 076601 (2018).
137. I. Eshghi, A. Zidovska, A. Y. Grosberg, Activity-driven phase transition causes coherent flows of chromatin. *Phys. Rev. Lett.* **131**, 048401 (2023).
138. L. Lizana, N. Nahali, Y. B. Schwartz, Polycomb proteins translate histone methylation to chromatin folding. *J. Biol. Chem.* **299**, 105080 (2023).
139. S. Baldi, D. S. Jain, L. Harpprecht, A. Zabel, M. Scheibe, F. Butter, T. Straub, P. B. Becker, Genome-wide rules of nucleosome phasing in drosophila. *Mol. Cell* **72**, 661–672.e4 (2018).
140. T. Raveh-Sadka, M. Levo, U. Shabi, B. Shany, L. Keren, M. Lotan-Pompan, D. Zeevi, E. Sharon, A. Weinberger, E. Segal, Manipulating nucleosome disfavoring sequences allows fine-tune regulation of gene expression in yeast. *Nat. Genet.* **44**, 743–750 (2012).
141. M. Galloni, H. Gyurkovics, P. Schedl, F. Karch, The bluetail transposon: Evidence for independent cis-regulatory domains and domain boundaries in the bithorax complex. *EMBO J.* **12**, 1087–1097 (1993).
142. D. G. Lupianez, K. Kraft, V. Heinrich, P. Krawitz, F. Brancati, E. Klopocki, D. Horn, H. Kayserili, J. M. Opitz, R. Laxova, F. Santos-Simarro, B. Gilbert-Dussardier, L. Wittler, M. Borschiwer, S. A. Haas, M. Osterwalder, M. Franke, B. Timmermann, J. Hecht, M. Spielmann, A. Visel, S. Mundlos, Disruptions of topological chromatin domains cause pathogenic rewiring of gene-enhancer interactions. *Cell* **161**, 1012–1025 (2015).
143. S. Rajderkar, I. Barozzi, Y. Zhu, R. Hu, Y. Zhang, B. Li, A. Alcaina Caro, Y. Fukuda-Yuzawa, G. Kelman, A. Akeza, M. J. Blow, Q. Pham, A. N. Harrington, J. Godoy, E. M. Meky, K. von Maydell, R. D. Hunter, J. A. Akiyama, C. S. Novak, I. Plajzer-Frick, V. Afzal, S. Tran, J. Lopez-Rios, M. E. Talkowski, K. C. K. Lloyd, B. Ren, D. E. Dickel, A. Visel, L. A. Pennacchio, Topologically associating domain boundaries are required for normal genome function. *Commun. Biol.* **6**, 435 (2023).
144. I. Williamson, L. Kane, P. S. Devenney, I. M. Flyamer, E. Anderson, F. Kilanowski, R. E. Hill, W. A. Bickmore, L. A. Lettice, Developmentally regulatedShhexpression is robust to TAD perturbations. *Development* **146**, dev179523 (2019).
145. D. Dorsett, The Many Roles of Cohesin in Drosophila Gene Transcription. *Trends Genet.* **35**, 542–551 (2019).
146. D. Dorsett, I. D. Krantz, On the molecular etiology of Cornelia de Lange syndrome. *Ann. N. Y. Acad. Sci.* **1151**, 22–37 (2009).
147. E. Ing-Simmons, R. Vaid, X. Y. Bing, M. Levine, M. Mannervik, J. M. Vaquerizas, Independence of chromatin conformation and gene regulation during Drosophila dorsoventral patterning. *Nat. Genet.* **53**, 487–499 (2021).
148. Y. Ghavi-Helm, A. Jankowski, S. Meiers, R. R. Viales, J. O. Korbel, E. E. M. Furlong, Highly rearranged chromosomes reveal uncoupling between genome topology and gene expression. *Nat. Genet.* **51**, 1272–1282 (2019).
149. A. Hafner, M. Park, S. E. Berger, S. E. Murphy, E. P. Nora, A. N. Boettiger, Loop stacking organizes genome folding from TADs to chromosomes. *Mol. Cell* **83**, 1377–1392.e6 (2023).
150. G. Ren, W. Jin, K. Cui, J. Rodrigez, G. Hu, Z. Zhang, D. R. Larson, K. Zhao, CTCF-mediated enhancer-promoter interaction is a critical regulator of cell-to-cell variation of gene expression. *Mol. Cell* **67**, 1049–1058.e6 (2017).
151. P. A. Clow, M. Du, N. Jillette, A. Taghbalout, J. J. Zhu, A. W. Cheng, CRISPR-mediated multiplexed live cell imaging of nonrepetitive genomic loci with one guide RNA per locus. *Nat. Commun.* **13**, 1871 (2022).
152. The ENCODE Project Consortium, An integrated encyclopedia of DNA elements in the human genome. *Nature* **489**, 57–74 (2012).
153. T. G. Kahn, E. Dorafshan, D. Schultheis, A. Zare, P. Stenberg, I. Reim, V. Pirrotta, Y. B. Schwartz, Interdependence of PRC1 and PRC2 for recruitment to Polycomb Response Elements. *Nucleic Acids Res.* **44**, 10132–10149 (2016).
154. J. T. Robinson, D. Turner, N. C. Durand, H. Thorvaldsdottir, J. P. Mesirov, E. L. Aiden, Juicebox.js provides a cloud-based visualization system for hi-c data. *Cell Syst.* **6**, 256–258.e1 (2018).

Acknowledgments: We are grateful to J. Smrek for discussions of the polymer mixing. **Funding:** The research in Y.B.S. laboratory is supported by grants from Cancerfonden (22 2285 Pj), Swedish Research Council (2021-04435), Kempestiftelserna (JCK22-0055), and Biotechnology Grant for Basic Research (Medical Faculty, Umeå University). The research in L.L. laboratory is supported by the Swedish Research Council (2021-04080).
Author contributions: Conceptualization: L.L. and Y.B.S. Writing—original draft: L.L. and Y.B.S. Writing—review and editing: L.L. and Y.B.S. **Competing interests:** The authors declare that they have no competing interests. **Data and materials availability:** All data needed to evaluate the conclusions in the paper are present in the paper and/or the materials cited herein.

Submitted 7 November 2023
Accepted 6 March 2024
Published 10 April 2024
10.1126/sciadv.adm8167